Tip-sample capacitance in capacitance microscopy of dielectric films

doi: 10.1063/1.368617

Tip–sample capacitance in capacitance microscopy of dielectric films

Kazuya Goto[a] and Kazuhiro Hane
Department of Mechatronics and Precision Engineering, Tohoku University, Sendai 980-8579, Japan

(Received 31 March 1998; accepted for publication 17 July 1998)

The tip–sample capacitance in the scanning capacitance microscopy (SCM) of dielectric films is described through theoretical calculations based on the method of images. The results are explained with the charge density distribution in the tip–sample system. Furthermore, capacitance signals in the tapping mode SCM of dielectric films are experimentally investigated and found to be in good agreement with the simulation results. © *1998 American Institute of Physics.* [S0021-8979(98)05820-4]

I. INTRODUCTION

Scanning capacitance microscopy (SCM)[1–7] is a technique to measure spatial variations of the tip–sample capacitance with a conductive tip. The SCM has been successfully applied to measurements of dopant density profiles in semiconductor devices on the basis of the conventional capacitance–voltage ($C-V$) method.[4] Another interesting application of the SCM is its use in the high-density information storage with a nitride–oxide–silicon medium.[5–7]

For interpretation of SCM images, it is essential to investigate the contrast formation and the quantitative determination of the tip–sample capacitance. Owing to the long-distance nature of capacitance, however, these problems are complicated and should be studied with theoretical support. So far, a number of theoretical studies have been reported concerning capacitance, electrostatic force, and its gradient in the tip–sample system.[2,8–11] The calculation methods used in the studies include the method of images,[2,12,13] the charge simulation method,[8,9] the surface charge method,[10] and the finite element method.[11] Most of the studies were made for conducting samples. Investigations of the SCM, however, should be performed for dielectric thin films with conductive substrates, because such samples are generally measured by the SCM. Recently, electrostatic calculations for SCM samples of dielectric films were performed with the finite element method, and the contrast formation in the SCM was discussed.[11]

In this article, we present the theoretical calculations and experimental measurements of the tip–sample capacitance for dielectric films with conductive substrates. The theoretical analyses are performed by using the method of images.[2,12,13] The dependence of the tip–sample capacitance on the tip–sample distance, the film thickness, and the film permittivity is investigated. Furthermore, capacitance signals in the tapping mode SCM[6,7] are calculated. They are compared with experimental results obtained in the tapping mode SCM of dielectric films with different thicknesses.

[a]Research Fellow of the Japan Society for the Promotion of Science.

II. THEORETICAL APPROACH BY THE METHOD OF IMAGES

A. Modeling of the tip–sample system

The tip–sample model for our electrostatic calculations is depicted in Fig. 1. The tip is represented by a conductive sphere with radius a, which equals the radius of curvature for the end of an actual tip. The tip end is away from the sample surface by the distance d. The sample is a dielectric film of thickness b having an underlying conducting plane. The permittivity of the film is ϵ_1, while that of the surrounding atmosphere is ϵ_0, which is assumed to equal that of vacuum. The potential is set to V at the sphere; the tip–sample voltage is V, because the potential at the plane is zero. In our model, we assume that, for $d<a$, the electrostatic field near the tip end approximates that of an actual tip–sample system; according to Ref. 8, the tip–sample field at the tip end for $d<a$ is dependent solely on the radius of the tip end and almost independent of the overall tip shape. The approximation can be good also for the tip-sample capacitance changes (SCM signals), if the field changes are caused exclusively in a local region near the tip end. This will be confirmed later by calculating the charge density distribution on the surfaces of the tip and sample.

The field determined by the model is equivalent to that determined by surface charges (space charges) continuously distributed over the surfaces of the sphere, film, and plane which are virtually replaced by vacuum (here, the surface charges on the film–plane interface are apparent charges, i.e., the real charges on the plane side plus the polarization charges on the film side). The surface charges are represented by the point charges obtained with the following technique. Electrostatic problems are then solved with the model by the use of the point charges.

B. Principle

The principle of the technique is to successively perform electrical imaging for the following three models: A point charge and a dielectric plane, a point charge and a conductive plane, and a point charge and a conductive sphere. The electrical imaging for these models is described in the literature.[13] The procedure for the technique is as follows. First, an initial charge is placed at the center of the sphere.

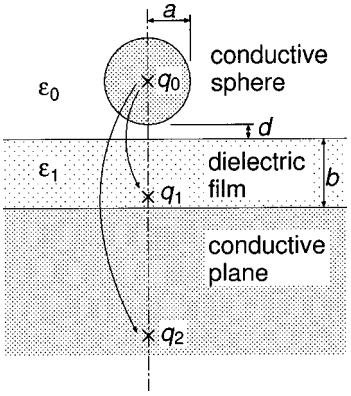

FIG. 1. Calculation model of the tip–sample system. ϵ_0 and ϵ_1 represent permittivities of the atmosphere (vacuum) and of the film, respectively. q_0 is the initial point charge. q_1 and q_2 are image charges in the dielectric film and the conductive plane, respectively.

The initial charge, shown as q_0 in Fig. 1, determines the potential V at the sphere. Here, $V=q_0/(4\pi\epsilon_0 a)$. Next, two image charges, shown as q_1 and q_2 in Fig. 1, are created from q_0. q_1 and q_2 are determined independently with the conventional methods[13] and placed in the film and the plane, respectively. (The location of q_1, the polarization charge, depends on from which side the charge is seen: It is located on the film side (as shown in Fig. 1) and at the same position as q_0, seen from the sphere and from the plane, respectively.) Likewise, two more image charges are created from each of q_1 and q_2. The production of image charges is continued in a similar manner until the total charges in the sphere and plane converge. The field determined by all the point charges (including the polarization charges) then approaches that determined by the surface charges mentioned above.

The tip–sample capacitance is given by dividing the total charges (real charges) by the tip–sample voltage V. Incidentally, calculating the density of the charges induced on the surfaces of the sphere and plane helps in understanding the tip–sample capacitance. The charge densities, which are proportional to the fields at the sphere and plane surfaces, are obtained by superimposing the fields from the point charges (including the polarization charges).

In order to simplify the calculations, the imaging operations in our computation method are performed by using an algorithm in which a charge in the sphere or plane generates an image charge in each of the sphere and plane. In other words, the imaging operations for an original charge and its polarization charge are performed simultaneously. In Fig. 1, for example, q_0 directly generates one image charge in the sphere and the other in the plane: The former is one image charge for q_1 and the latter is the sum of q_2 and the other image charge for q_1.[13]

C. Simulation of capacitance signals in tapping mode SCM

It is interesting to compare tip–sample capacitances obtained by the above technique with corresponding experimental results. In particular, the comparison should be performed in terms of capacitance changes reflecting changes in the field near the tip end. Accordingly, the experiment should be performed with an SCM using a capacitance modulation technique for differential capacitance sensing.[2–6] The tapping mode SCM[6,7] is a good choice here. This SCM uses the tapping motion of the tip not only to modulate the tip–sample capacitance but also to accurately control the tip–sample distance in a tapping mode scanning force microscopy fashion. Simulations of capacitance signals in the tapping mode SCM are performed in the following way. The tip–sample distance d is sinusoidally changed due to the sinusoidal vibration of the tip tapping the sample surface at frequency f. $d(t)$ as a function of time t is then given by $d(t)=d_{\max}(1-\cos 2\pi ft)/2$, where $d_{\max}$ is the maximum tip–sample distance, i.e., the peak-to-peak amplitude of the tip vibration. The tip–sample capacitance $C(d)$ as a function of d is accordingly modulated with the tip vibration and then lock-in amplified. Consequently the output signal is proportional to C_{mod}, the component oscillating at the fundamental frequency (modulation frequency) of f. C_{mod} is given by

$$C_{\mathrm{mod}}=\frac{2}{T}\int_{-T/2}^{T/2} C[d(t)]\cos 2\pi ft\, dt, \tag{1}$$

where $T=1/f$.

D. Calculations

The electrostatic calculations by the above method require that the tip–sample fields should converge after a certain number of imaging operations. In order to confirm the convergence, the total charges obtained after n times of imaging operations were examined. One imaging operation defined here is to produce, in the algorithm mentioned above, two image charges from every original charge: In the nth operation, 2^n image charges are produced from 2^{n-1} original charges. The calculations were performed for $a=100$ nm, $b=50$ nm, $\epsilon_r=\epsilon_1/\epsilon_0=5$, and $d=0$ nm. In the following calculations, $a=100$ nm and $\epsilon_r=5$ unless otherwise specified.

Tip–sample capacitances were calculated as functions of d for $b=50$ and 100 nm and $a=50$, 100, and 150 nm. d was varied from 0 to 100 nm. Next, the dependence of the tip–sample capacitance on the thickness and the permittivity of a film was examined for $d=0$ nm. b and ϵ_r were varied from 2 to 200 nm and from 1 to 20, respectively. Furthermore, the charge densities on the surfaces of the sphere and plane were calculated for $d=0$ and 50 nm and $b=50$ nm; for $b=25$, 50, and 100 nm and $d=0$ nm; and for $\epsilon_r=2.5$, 5, and 10, $b=50$ nm, and $d=0$ nm.

Capacitance signals in the tapping mode SCM were calculated according to Eq. (1) for $b=50$ and 100 nm while $a=50$, 100, and 150 nm. $d_{\max}$ was varied from 0 to 100 nm. Capacitance curves for $C(d)$ were obtained by calculating tip–sample capacitances for different values of d and then interpolating the calculated values.

III. EXPERIMENT

As mentioned above, the tip–sample capacitance in the SCM of dielectric films on conductive substrates was investigated experimentally with the tapping mode SCM.[6,7] The

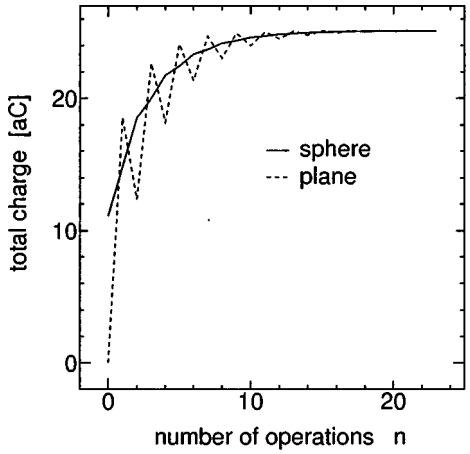

FIG. 2. Convergence of the total charges in the sphere and the plane. $b=50$ nm, $\epsilon_r=5$, and $a=100$ nm.

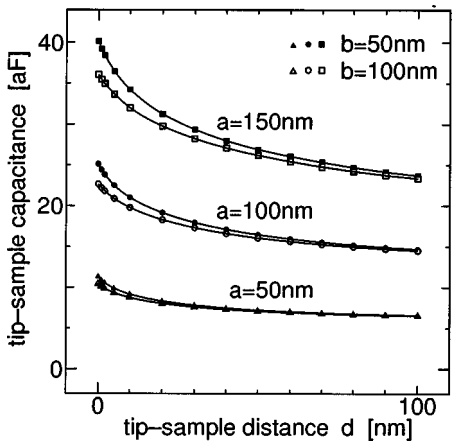

FIG. 3. Tip–sample capacitance as a function of the tip–sample distance d for $\epsilon_r=5$.

samples used here are thermally grown SiO_2 films on Si wafers [n-type, (100), 0.01–0.02 Ω cm]. The Si substrates are regarded as conductors because of their very high dopant density. The SiO_2 films were etched with hydrogen fluoride (HF) solution to form 5 μm line/space structures having two different film thicknesses. Two SiO_2/Si samples were used in the SCM measurements; sample A with $b=240$ and 120 nm, and sample B with $b=240$ and 50 nm.

The experimental setup here was the same as that previously used.[6,7] The probe is a cantilever of tungsten wire of 50 μm in diameter. The cantilever length is about 2 mm. The free end of the probe is bent at a right angle, with the tip length less than 1 mm. The end of the tip is sharpened by electrochemical etching. According to a scanning electron microscopy observation, the whole tip can be represented by a cone with a spherical end. The half opening angle for the cone is about 15°. The tip end is well represented by a sphere with the radius of 200 nm in terms of the tip size, although, strictly speaking, the radius of curvature at the apex is about 400 nm.

The samples were line scanned by the tapping mode SCM, while the capacitance signal and the topographic signal were simultaneously acquired with tapping motion amplitudes kept constant by feedback control. The scan speed was set very low (10 s/line) so that the feedback controller could follow step changes in a sample with sufficiently small errors. $d_{\max}$ was set to different values ranging from 30 to 100 nm. The experimental results were then compared with theoretical results obtained by the above method.

IV. RESULTS AND DISCUSSION

A. Calculation results

In Fig. 2, the total charges (real charges) in the sphere and plane for $b=50$ nm, $\epsilon_r=5$, and $a=100$ nm are shown as functions of the number of operations n. The tip–sample voltage V is 1 V. Figure 2 shows that the convergence of the total charges is quite good. The convergence tends to be slower for thinner films or higher permittivity films.

Figure 3 shows tip–sample capacitances as functions of d for $b=50$ and 100 nm and $\epsilon_r=5$. As shown in Fig. 3, the capacitances do not change much with changes in the tip–sample distance or the film thickness, unlike a simple parallel-plate capacitance. Also, with the increase of the tip–sample distance, the tip–sample capacitances do not approach zero but $C=4\pi\epsilon_0 a$, the capacitance for an isolated conductive sphere with radius a.

Figure 4 shows the capacitance–thickness curve for $\epsilon_r=5$ and capacitance–permittivity curve for $b=50$ nm. As exhibited in Fig. 4, the capacitance varies slowly with changes in the thickness and permittivity, showing, roughly speaking, logarithmic dependence on them. This is an important result for interpretations of SCM images.

Figure 5 shows surface charge density distributions on the conductive sphere and plane for $a=100$ nm. The tip–sample voltage V is 1 V. Figures 5(a) and 5(b) show the charge densities on the sphere and plane, respectively. Here, $d=0$ and 50 nm while $b=50$ nm and $\epsilon_r=5$. The tip–sample capacitances are 25.1 and 16.5 aF for $d=0$ and 50 nm, re-

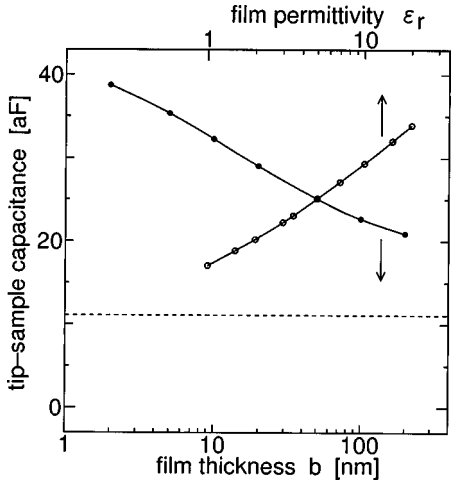

FIG. 4. Dependence of the tip–sample capacitance on the thickness b and the relative permittivity ϵ_r of the film for $a=100$ nm. $\epsilon_r=5$ for the capactance–thickness curve. $b=50$ nm for the capacitance–permittivity curve. The broken line is for $C=4\pi\epsilon_0 a$, the capacitance of an isolated conductive sphere.

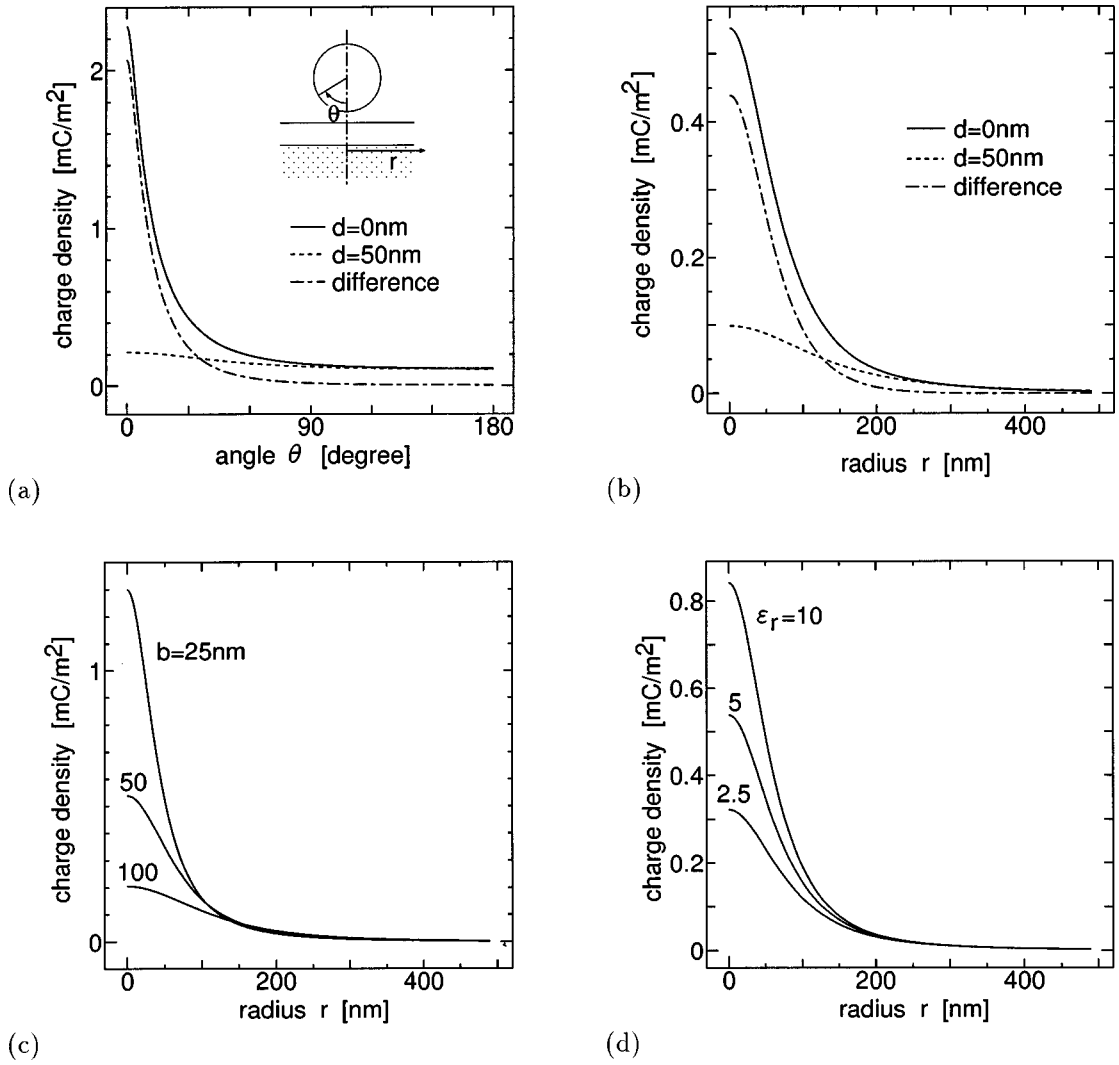

FIG. 5. Charge densities on the sphere (a) and on the plane (b) for $d=0$ and 50 nm, $a=100$ nm, and $\epsilon_r=5$; and charge densities for different film thicknesses (c) and for different permittivities (d).

spectively. Figure 5(c) shows charge densities on the plane for $b=25$, 50, and 100 nm while $d=0$ nm and $\epsilon_r=5$. The tip–sample capacitances are 28.0, 25.1, and 22.7 aF for $b=25$, 50, and 100 nm, respectively. Figure 5(d) shows charge densities on the plane for $\epsilon_r=2.5$, 5, and 10 while $b=50$ nm and $d=0$ nm. The tip–sample capacitances are 21.3, 25.1, and 29.4 aF for $\epsilon_r=2.5$, 5, and 10, respectively. As shown in Fig. 5, the charge densities are concentrated on the center axis ($r=0$ and $\theta=0$) of the tip–sample system and the charge density changes are almost zero for large values of θ and r. Furthermore, the broadening of the charge density distribution, evaluated by half width at half maximum (HWHM), decreases with the decrease of d and b and with the increase of ϵ_r, while the maximum value of the density increases. These facts account for the changes in the tip–sample capacitance being small, as discussed above with respect to Figs. 3 and 4. In addition, the broadening of the charge density distributions on the plane is likely to determine the lateral resolution in the SCM. In Fig. 5(b), the HWHM of the curve for the charge density difference is comparable to the tip radius, which suggests that the lateral resolution in the SCM is comparable to the tip size.[2,3,6]

The surface integral of the charge density change shown in Fig. 5(a) proves that the change in the surface charges on the area defined by $0°<\theta<90°$, the hemisphere on the sample side, are responsible for 95% of the change in the total charge in the sphere. This fact supports, in terms of the capacitance change, the validity of the approximation that an actual tip is represented with a sphere. A condition for good approximation will be $d<a$, as mentioned in Sec. II.

Figure 6 shows the simulation results of the capacitance signals in the tapping mode SCM of dielectric films of $b=50$ and 100 nm and $\epsilon_r=5$. In Fig. 6, curves for $2C_{\mathrm{mod}}$, the peak-to-peak amplitudes of the capacitance signal, are drawn as functions of $d_{\max}$. This figure shows that the gradients of the curves decrease with $d_{\max}$, reflecting the gradients of the capacitance–distance curves shown in Fig. 3. In addition, the signal contrasts, i.e., the ratios of the signals for $b=50$ nm to those for $b=100$ nm, do not depend considerably on $d_{\max}$ or a.

B. Experimental results

Figure 7(a) shows a cross section of a SiO_2 sample (sample A). Figure 7(b) shows the capacitance signal and the

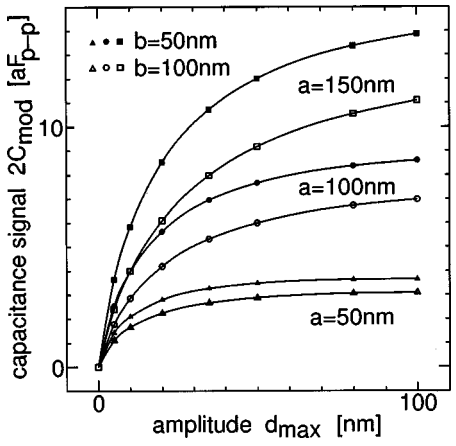

FIG. 6. Simulation results for capacitance signals of $2C_{\mathrm{mod}}$ in the tapping mode SCM as functions of the amplitude d_{max} of the tapping motion of the tip. $\epsilon_r = 5$.

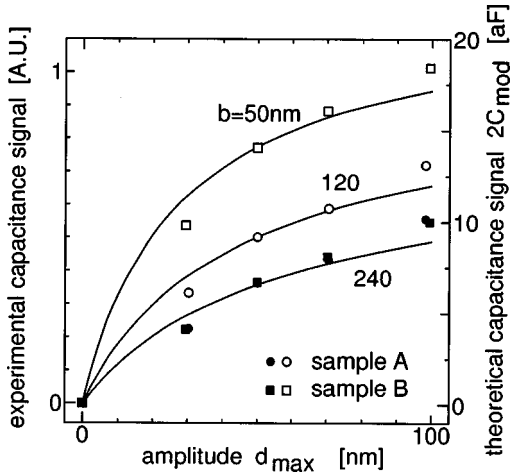

FIG. 8. Experimental data plots and the corresponding theoretical curves for capacitance signals obtained from samples A and B in the tapping mode SCM.

topographic signal obtained simultaneously from sample A for $d_{\mathrm{max}} = 50$ nm by line scanning a region having a step, the thickness difference. As shown in Fig. 7(b), the capacitance signal for $b = 120$ nm is larger than that for $b = 240$ nm by a factor of 1.4. In addition, in Fig. 7(b), the capacitance signal drops in a region ($b = 240$ nm) on the right side of the step edge. This means that the step changed the tip–sample capacitance, reflecting its long-distance nature. The width designated in Fig. 7(b) probably reflects the broadening of the charge density distribution on the sample. In fact, the width is comparable to the HWHM of the charge density distribution theoretically calculated.

The capacitance signals for different film thicknesses are plotted against d_{max} as shown in Fig. 8. (The capacitance signals from sample B for $b = 240$ nm were smaller than those from sample A by about 10%, which is often the case when samples are changed. Hence all the capacitance signals from sample B were corrected; namely, they are multiplied by a constant, assuming that the tip–sample capacitance changes with samples A and B for $b = 240$ nm had been the same.) The theoretical curves corresponding to the experimental data are also drawn in Fig. 8. These curves are obtained for $a = 200$ nm and $\epsilon_r = 3.7$, the permittivity of the thermally grown SiO_2. The experimental data are plotted so that those for $d_{\mathrm{max}} = 50$ nm fit the curves well. As a whole, the experimental results agree well with the theoretical results as shown in Fig. 8, which is especially true for the relative values of the capacitance signals for different film thicknesses. The agreement verifies that most of the charge density change is caused in a local region near the tip end, i.e., if the contribution from regions far from the tip end is large, the signal contrasts would be considerably reduced. In addition, theoretical signals were also calculated for $a = 400$ nm. Each of the curves for these signals could be better fit to the corresponding experimental data, but the signal contrasts were greater than those for the data. A possible reason for the small discrepancy between the theoretical and experimental results is that the end of the tip used in the experiment was not perfectly spherical. Another reason is that, in principle, the actual tip–sample field cannot be completely realized by the presented model, even if the tip end is perfectly spherical.

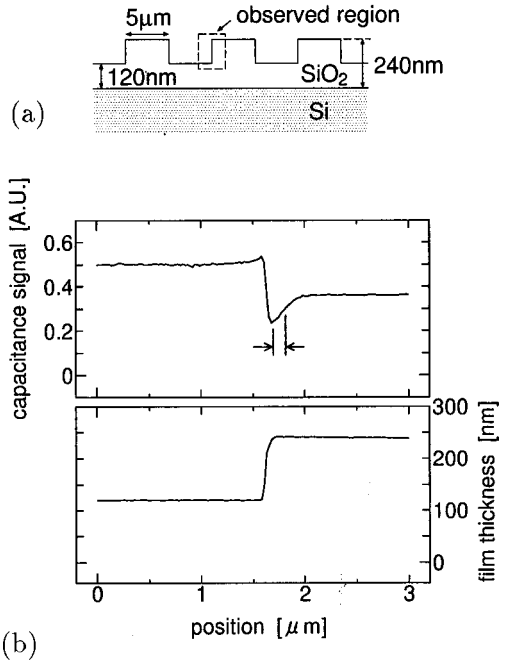

FIG. 7. (a) Cross section of a SiO_2 sample (sample A); (b) the capacitance signal and the topographic signal obtained in the experiment with the tapping mode SCM for $d_{\mathrm{max}} = 50$ nm.

More strict comparisons between the experimental and theoretical results are possible, provided that the absolute values for the former are obtained. For this purpose, accurate calibration of the tip–sample capacitance sensing is indispensable, although it is difficult because the capacitances to be detected are very small compared to stray capacitances. In our experiments, the magnitudes of the experimental capacitance signals ($2C_{\mathrm{mod}}$) roughly calibrated proved to be of the same order as those of the theoretical signals.

V. CONCLUSIONS

The tip–sample capacitance in the SCM was investigated for samples of dielectric films on conductive sub-

strates. The method of images was applied to electrostatic calculations for the tip–sample system represented by a sphere-film-plane structure. It proved that the tip–sample capacitance changes slowly with the tip–sample distance, film thickness, and the film permittivity, as opposed to a simple parallel-plate capacitance. The capacitance increase being small is a result of the concentration of the charge density distribution on the center axis of the tip–sample system. Capacitance signals in the tapping mode SCM were theoretically calculated from capacitance–distance curves obtained. The simulation results agreed well with the experimental results for SiO_2/Si samples.

ACKNOWLEDGMENTS

This work was supported in part by a Grant-in-Aid from the Ministry of Education, Science, and Culture of Japan, by Support Center for Advanced Telecommunications Technology Research, and by Hoso Bunka Foundation. Part of the work was performed in Venture Business Laboratory in Tohoku University.

[1] J. R. Matey and J. Blanc, J. Appl. Phys. **57**, 1437 (1985).
[2] H. P. Kleinknecht, J. R. Sandercock, and H. Meier, Scanning Microsc. **2**, 1839 (1988).
[3] C. C. Williams, W. P. Hough, and S. A. Rishton, Appl. Phys. Lett. **55**, 203 (1989).
[4] C. C. Williams, J. Slinkman, W. P. Hough, and H. K. Wickramasinghe, Appl. Phys. Lett. **55**, 1662 (1989).
[5] R. C. Barrett and C. F. Quate, J. Appl. Phys. **70**, 2725 (1991).
[6] K. Goto and K. Hane, Rev. Sci. Instrum. **68**, 120 (1997).
[7] K. Goto and K. Hane, *Advances in Information Storage Systems* (American Society of Mechanical Engineers, World Scientific, Singapore).
[8] G. Mesa, E. Dobado-Fuentes, and J. J. Sáenz, J. Appl. Phys. **79**, 39 (1996).
[9] S. Belaidi, P. Girard, and G. Leveque, J. Appl. Phys. **81**, 1023 (1997).
[10] S. Watanabe, K. Hane, T. Ohye, M. Ito, and T. Goto, J. Vac. Sci. Technol. B **11**, 1774 (1993).
[11] Š. Lányi, J. Török, and P. Řehůřek, J. Vac. Sci. Technol. B **14**, 892 (1996).
[12] H. C. Miller, J. Appl. Phys. **37**, 784 (1966).
[13] W. K. H. Panofsky and M. Phillips, *Classical Electricity and Magnetism*, 2nd ed. (Addison–Wesley Reading, MA, 1962), Chap. 3; K. J. Binns and P. J. Lawrenson, *Analysis and Computation of Electric and Magnetic Field Problems*, 2nd ed. (Pergamon, Oxford, 1973), Chap. 3.